Raman spectroscopy for medical diagnostics — From in-vitro biofluid assays to in-vivo cancer detection ☆

Kenny Kong [a], Catherine Kendall [b,c], Nicholas Stone [b,c], Ioan Notingher [a,*]

[a] School of Physics and Astronomy, University of Nottingham, University Park, Nottingham NG7 2RD, United Kingdom
[b] University Exeter, College of Engineering Mathematics and Physical Science, Exeter, Devon EX4 4QL, United Kingdom
[c] Gloucestershire Hospital NHS Foundation Trust, Biophotonic Research Unit, Gloucester GL1 3NN, United Kingdom

ARTICLE INFO

ABSTRACT

Raman spectroscopy is an optical technique based on inelastic scattering of light by vibrating molecules and can provide chemical fingerprints of cells, tissues or biofluids. The high chemical specificity, minimal or lack of sample preparation and the ability to use advanced optical technologies in the visible or near-infrared spectral range (lasers, microscopes, fibre-optics) have recently led to an increase in medical diagnostic applications of Raman spectroscopy. The key hypothesis underpinning this field is that molecular changes in cells, tissues or biofluids, that are either the cause or the effect of diseases, can be detected and quantified by Raman spectroscopy. Furthermore, multivariate calibration and classification models based on Raman spectra can be developed on large "training" datasets and used subsequently on samples from new patients to obtain quantitative and objective diagnosis. Historically, spontaneous Raman spectroscopy has been known as a low signal technique requiring relatively long acquisition times. Nevertheless, new strategies have been developed recently to overcome these issues: non-linear optical effects and metallic nanoparticles can be used to enhance the Raman signals, optimised fibre-optic Raman probes can be used for real-time in-vivo single-point measurements, while multi-modal integration with other optical techniques can guide the Raman measurements to increase the acquisition speed and spatial accuracy of diagnosis. These recent efforts have advanced Raman spectroscopy to the point where the diagnostic accuracy and speed are compatible with clinical use. This paper reviews the main Raman spectroscopy techniques used in medical diagnostics and provides an overview of various applications.

© 2015 The Authors. Published by Elsevier B.V. This is an open access article under the CC BY license (http://creativecommons.org/licenses/by/4.0/).

Contents

☆ This review is part of the *Advanced Drug Delivery Reviews* theme issue on "Pharmaceutical applications of Raman spectroscopy - from diagnosis to therapeutics".
 * Corresponding author.
   E-mail address: ioan.notingher@nottingham.ac.uk (I. Notingher).

1. Introduction

Raman spectroscopy is a powerful analytical technique that can measure the chemical composition of complex biological samples, such as biofluids, cells and tissues. A Raman spectrum represents a molecular fingerprint of the sample and provides quantitative information regarding its chemical makeup. Biochemical changes in cells and tissues, that may either be caused or are the cause of a disease, can lead to significant changes in the Raman spectra. The potential of Raman spectroscopy arises from its ability to detect such biochemical changes at a molecular level, and therefore, can be used for diagnostics, prognostics or as a tool for evaluating new therapies.

Raman spectroscopy has several features that are advantageous for medical diagnostics. It has high chemical specificity and molecular information can be obtained without requiring staining or labelling. Changes in the molecular composition of biological samples as measured by Raman spectroscopy can be used to build multivariate calibration and classification models, which allow quantitative and objective diagnosis for independent patients. Raman spectroscopy relies on scattering of light by molecules and information regarding the vibrational modes of the molecules can be obtained using visible or near-infrared lasers. Thus, Raman spectroscopy can take advantage of the advanced optical microscopy technologies, optical fibres, miniaturised lasers and other photonic devices, to improve diagnostic performance and speed. Often the measurements are carried out in back-scattering geometry without requiring transmission of light through the specimen. This feature is useful in particular for in-vivo diagnostic and for examination of thick tissue specimens (e.g. surgical resections), without requiring micro-sectioning. The use of visible or near-infrared light for excitation also reduces the absorption effects of water, allowing measurements of body fluids or cells within water environments.

Similar to other optical techniques, Raman spectroscopy can provide real-time (or near real-time) molecular information and high-resolution imaging at relatively low cost compared to other well-established medical imaging techniques (e.g. ultrasound, magnetic resonance imaging, etc.). This is an important feature as often the clinical implementation and translation of technologies are limited by practical, logistical and financial factors.

One of the main draw-backs of Raman spectroscopy, that so far has partly limited the translation into the clinic, is the relatively low efficiency of the inelastic light scattering compared to elastic scattering, fluorescence emission or absorption of infrared light. The low Raman signals have often limited the speed of the technique. Compromises to reduce acquisition times can decrease diagnosis accuracy when spectra are acquired with insufficient signal-to-noise ratios, or with spatial under-sampling. Nevertheless, new strategies have been recently developed to address this limitation: imaging modalities based on non-linear Raman scattering, multimodal integration and selective-sampling Raman microscopy, the use of nanomaterials and photonic structures to enhance the Raman signals, fibre-optics probes for hand-held diagnostic devices and endoscopes, spatially-offset and needle-probes for deep and subsurface diagnostics. These developments have made important steps toward maximising the diagnostic accuracy and speed, and often rely on cost-effective solutions that are likely to be adopted into the healthcare services.

This paper reviews the main Raman spectroscopy techniques used for biomedical diagnostics and provides an overview of applications, including biofluids, cells and tissues. The article does not aim to be a complete record of all papers in this research area, but instead focuses on selected papers that emphasise recent advances or define new trends in the field. Section 2 describes the main Raman spectroscopy techniques, including methods for spectral imaging of cells and tissue. Section 3 presents diagnostics examples of tissue samples, in-vivo and ex-vivo imaging, in-vivo diagnosis based on hand-held fibre probes and SORS. Section 4 focuses on Raman spectroscopy assays for biofluid analysis, including blood, saliva, urine and tear samples.

2. Raman spectroscopy techniques

2.1. Raman micro-spectroscopy

The use of excitation lasers with wavelengths in the visible and near-infrared regions permits efficient coupling of Raman spectrometers with optical microscopes [1]. Such Raman micro-spectrometers allow mapping of the molecular properties of the samples with diffraction-limited spatial resolution (300–500 nm). The most common method for obtaining Raman spectral images is by raster-scanning the sample through the laser spot (or scanning the laser spot across the sample) and then applying a uni- or multivariate spectral model to each Raman spectrum. Raman spectral imaging based on line-mapping [2] (i.e. laser beam expanded to form a line spot on the sample surface) can considerably decrease the imaging time compared to single-point raster-scanning, up to a factor equal to the number of simultaneously-measured sampling points, provided the laser power used for single-point mapping can be maintained over the whole laser line. Recent studies have demonstrated that an increase of a factor of 10 can realistically be achieved for imaging tissue samples, compared to point-by-point scanning [3]. More recently, multifocal Raman micro-spectrometers based on diffractive optical elements [4] or spatial light modulators [5] have been proposed for simultaneous read-out of multiple Raman spectra. Shuttering systems using different masks or arrays of optical fibres were used to couple the microscope to the Raman spectrometer by matching the pattern of the laser beams on the sample to the fibre/slit pattern. If only uni-variate Raman models are used, the speed of Raman spectral imaging can be significantly increased by wide-field Raman microscopy: the laser is expanded to illuminate the entire area of the sample and the scattered Raman light corresponded to selected wavenumbers are imaged on a CCD [6]. This approach may be difficult in applications where variations in the baseline of Raman spectra may often obscure the small differences in the Raman bands used for discrimination in the diagnostic model.

2.2. Selective-sampling Raman micro-spectroscopy

In many medical applications, for example the assessment of resection margins during cancer surgery, it is desirable to obtain high-spatial resolution Raman spectral images for large samples (e.g. 1–5 cm). In such cases, the techniques based on raster-scanning are often not suitable because of the long data acquisition time required for recording the datasets of Raman spectra. For example, achieving

Raman spectral images for a 1 cm × 1 cm tissue sample at a spatial resolution of ~20 μm, requires typically acquisition times of one day (~5 h per 1 mm^2) [7–9]. In selective sampling, information regarding the spatial features of the sample, either measured by an alternative optical technique [7,10] or estimated in real-time from the Raman spectra [11,12], can be used to reduce the number of Raman spectra by more than two orders of magnitude.

The first approach developed by Rowlands et al. [13] estimated the main features of the sample in real-time; the next sampling point for Raman spectroscopy is selected as the location with the maximum absolute difference between two interpolating surfaces for the already measured Raman spectra. In regions of the sample with few spatial features, the two interpolants should converge on the same result. However, in the regions with a higher level of spectral variation, the difference between the two interpolants provides an indication of the optimal point to measure next. In this way, the algorithm samples regions of uncertainty with high resolution, at the expense of regions containing relatively few spatial features. The feasibility of using this selective sampling method for imaging cells and tissues has been demonstrated [10–12]. A different approach for determining the optimal positions of the sampling points for Raman spectroscopy is to use a much faster alternative imaging technique that has high sensitivity to the features of interest but not necessarily high specificity; these features of interest are then used to generate and prioritise the sampling points for Raman spectroscopy [7]. The key advantages of this approach are: i) reduced number of Raman spectra, hence fast data acquisition and processing and ii) the spatial-resolution is not compromised by the reduced number of Raman spectra because resolution is determined by the alternative optical technique used to establish the spatial features of the sample (e.g. confocal fluorescence microscopy [6]).

2.3. Coherent anti-Stokes Raman spectroscopy (CARS) and stimulated Raman spectroscopy (SRS)

Spontaneous Raman scattering, which relies on a single excitation laser beam, is an incoherent phenomenon because the molecular vibrations in a sample are not correlated. Coherent Raman spectroscopy techniques rely on non-linear effects to increase the speed and spatial resolution of Raman spectroscopy by inducing coherent molecular vibrations in the sample. Coherent anti-Stokes Raman spectroscopy (CARS) uses a "pump" laser (frequency ν_p) and a "Stokes" laser (frequency ν_S) to drive coherent vibrations of the molecules at selected frequencies (frequency ν_{vib}). Typically, one laser frequency is fixed at ν_S and the other is tuned to ν_p to excite the molecular vibrational mode of interest at a frequency $\nu_{vib} = \nu_p - \nu_S$. In this process, three photons are absorbed, two "pump" photons and one "Stokes" photon, and the signal corresponding to "anti-Stokes" photons of frequency $\nu_{AS} = 2\nu_p - \nu_S$ is detected to create the CARS images. CARS has been mostly used to image cells and tissues by exciting the CH stretching vibrations (2600–3000 cm^{-1}) in lipids and proteins [14]. Recently, broadband CARS techniques, in which multiple Raman transitions are probed simultaneously, have been extended in the fingerprint region to allow imaging of biological tissues with improved molecular contrast [15].

Stimulated Raman scattering (SRS) is based on only one "pump" and one "Stokes" photons. When the difference between the frequencies of the "pump" and "Stokes" photons match the frequency of a molecular vibrational mode $\nu_{vib} = \nu_p - \nu_S$, stimulated excitation of vibrational transitions occurs. In this case the "Stokes" beam experiences stimulated Raman gain while the pump beam experiences stimulated Raman loss. High-frequency modulation of either "Stokes" or "pump" beams can be used to detect the small beam intensity changes and generate high-speed images at selected vibrational frequencies. Compared to CARS, SRS is free of non-resonant background and high-speed images of cells and tissues have been reported [16]. Both CARS and SRS microscopy are based on non-linear optical effects, therefore the spatial-

resolution of these techniques are superior to spontaneous Raman micro-spectroscopy.

2.4. Surface enhanced Raman spectroscopy (SERS)

An alternative method to enhance the weak signals in spontaneous Raman spectroscopy is to use metallic nanostructures capable to provide surface enhanced Raman scattering [17]. When the molecules of interest are adsorbed or located in the vicinity of such a metallic nanostructure, enhancement of the Raman scattering occurs due to the resonant interaction of light with the surface plasmons excited at the surface of the structure (electromagnetic enhancement) [18,19]. This resonant interaction creates an enhanced electric field (10–100×) localised to a region of only few nanometres from the surface. This increase in the localised electric field subsequently can lead to a ~10^5–10^6 fold enhancement for the Raman bands for molecules located in the vicinity of the surface. An additional enhancement, chemical enhancement, can also be observed for molecules adsorbed at the surface of the nanostructure due to electronic interactions between the molecule and surface. Physio- or chemisorption perturbs the polarisability tensors of the molecules, leading to changes in the intensity of Raman bands [20]. In addition, resonant Raman scattering effects can be observed due to excitation into a charge-transfer transition [21]. Another strategy in SERS diagnostics is the use of tailored nanoparticles as markers conjugated with specific antibodies. The corresponding antibodies are labelled by SERS-active nanoparticles, comprising of metallic nanoparticles with chemisorbed Raman reporter molecules. The feasibility of this approach for tissue diagnostics has been demonstrated [22].

2.5. Spatially offset Raman spectroscopy (SORS) and transmission Raman spectroscopy (TRS)

Traditional Raman spectroscopy, when illuminating and collecting light from the same area, in tissues usually has a maximum penetration depth of a few hundred microns, thus, restricting analysis to the surface or near-surface area of samples. The development of spatially offset Raman spectroscopy (SORS) has enabled spectral measurements from volumes as deep as 10–20 mm into the sample. SORS involves collecting the scattered light away from the point of laser illumination [23,24]. With increasing spatial offset of the collection and the illumination points, measurements deeper in tissue are possible. Clinical applications of deep Raman techniques may include applications in urology, bone and breast disease [25–27].

Transmission Raman spectroscopy (TRS) is an extreme form of SORS, whereby the collection and illumination points are on opposite sides of the sample [28]. This approach is ideally suited for bulk analysis of opaque/turbid materials and has been shown to be feasible through a many millimetres of tissues. Despite the sample being opaque, light from the laser can pass through the sample via light scattering processes and many of these photons contain Raman information, and thus transmission Raman spectroscopy is feasible. Applications to breast cancer diagnosis have been investigated [29].

The combination of the powerful techniques of SERS and SORS has led to the development of the novel approach of surface enhanced spatially offset Raman spectroscopy (SESORS). To date it has been demonstrated that the presence and location of up to 4 labelled nanoparticles can be measured through tissue thicknesses of between 20 and 50 mm [30,31]. Bisphosphonate-bone functionalization [32] and glucose sensing [33] have also been demonstrated.

2.6. Fibre-optic Raman probes

Raman spectroscopy is suitable for use with fibre-optic probes, making it potentially ideal as a medical diagnostic tool for assessment of hollow organs. Fibre-optic probes designed for in vivo use must

overcome signal-to-noise ratio challenges, and face the major problem of Raman signals and photoluminescence generated in the laser delivery fibres themselves. For certain applications, all this must be achieved with a probe of very small size to enable access to body cavities, and in a sufficiently short time to allow accurate measurement from a moving target organ [24–27]. Furthermore, spectral sampling volumes can be critical for accurate identification of early disease in certain conditions such as dysplasia, when probing for early disease close to the surface of an organ [26,27]. Further miniaturisation can allow measurement of Raman signals through needles (see Fig. 1) and thus allow access to solid organs such as lymph nodes, prostate and breast [34–38].

To avoid the intense background signal generated in the fused-silica fibres in the fingerprint region (600–1800 cm^{-1}), some fibre-optic Raman probes have been developed to work in the high-wavenumber region (2400–3800 cm^{-1}) [29]. These probes can use a single fibre for guiding laser light to the sample and for collecting the Raman scattered light. This configuration has been demonstrated to provide high-quality high-wavenumber Raman spectra of tissue with almost no Raman background signal from the fibre [39]. An alternative method has been explored for filtering the elastically scattered laser line from the collection fibres and thus minimising the induction of background signal from fibres. This uses in-line fibre Bragg gratings (FBG) to reject/reflect the laser light in the collection path. A Raman probe was built consisting of one excitation fibre and six multicore single-mode fibres (19 cores) with inscribed FBGs as collection fibres [40].

3. In-vivo and in-vitro Raman diagnostics based on tissue analysis

3.1. Brain cancer

Around 45% of brain tumours are gliomas, which are currently diagnosed by a combination of CT scanning, magnetic resonance imaging and electroencephalogram, followed by surgical excision for definitive identification of pathology. Because often neoplastic tissue cannot be distinguished from healthy tissue during the surgery, one of the key challenges in brain tumour surgery is to delineate normal tissue from tumour in order to avoid neurologic deficit associated with damaging functional cerebral structures. On the other hand, incomplete removal of the tumour increases the risk of tumour recurrence.

Early work by Koljenovic et al. showed that fibre-optic Raman probes based on the high-wavenumber spectral region (2400–3800 cm^{-1}) can be used to characterise porcine brain tissue ex-vivo [41]. The measurement of the high-wavenumber spectral region avoids the background Raman scattering from silica fibres while still providing high-chemical specificity and diagnostic power [39,42]. The authors developed multivariate classification model (least-squares fitting) that allowed discrimination of brain structures based on the biochemical contrast. The Raman spectra of grey matter was characterised by high intensity bands associated with proteins, DNA, and phosphatidylcholine compared

Fig. 1. Raman needle probe, constructed using one illumination and one collection fibre, with appropriate spectral filtration included in the syringe body [28]. Reprinted with permission from Springer.

with white matter, while the spectra of white matter was dominated by spectral features corresponding to cholesterol, sphingomyelin, and galactocerebroside.

The potential of using a fibre-optic Raman probe for in-vivo diagnosis of brain tumours was investigated by Kirsch et al. [43]. Raman spectral maps over areas 3.6×3.2 mm^2 allowed label-free diagnosis of induced metastatic brain tumours in mice with accuracy of ~250 μm. [43]. Krafft et al. used Raman spectroscopy in the fingerprint region (600–1800 cm^{-1}) to investigate primary brain cell density [44]. For high-grade gliomas, the Raman spectra had higher contribution from nuclei acid compared to normal tissue. The authors also demonstrated the ability to create Raman spectral images by raster-scanning, which were in good correlation with the images obtained by H&E staining [45].

Spectral images of brain tissue with higher-spatial resolution have been reported using coherent Raman micro-spectroscopy techniques. CARS imaging tuned to probe C–H molecular vibrations was used to analyse human tumours (glioblastoma, brain metastases of melanoma and breast cancer) induced in an orthotopic mouse model [46]. As all brain tumours have significantly lower lipid content compared to the normal parenchyma, CARS images can clearly delineate the tumour borders and infiltrations. Ji et al. developed a technique based on SRS for real-time imaging guidance for brain tumour surgery [47]. SRS images obtained at 2930 and 2845 cm^{-1}, bands corresponding to lipids and proteins, allowed differentiation of tumour from nonneoplastic tissue in an infiltrative human glioblastoma xenograft mouse model (correlation between SRS and H&E images for glioma infiltration was k = 0.98). The technique was also used in-vivo during surgery on mice to image tumour margins that were undetectable under standard operative conditions (Fig. 2).

Medyukhina et al. have reported new algorithms for automated calculation of quantitative values (such as cell density, nucleus-to-cytoplasm ratio, average nuclear size) that can be used for objective diagnostic of brain tumours based on non-linear Raman microscopy [48]. Using co-registered two-photon excited fluorescence (TPEF) and CARS images of human brain tumour samples, the grayscale information was used to detect the location of the cell nuclei while the gradient information allowed delineation of the nuclear and cellular boundaries.

3.2. Breast cancer

Breast cancer is the second most common cancer and the most common cause of death from cancer among women [50]. In Europe, more than ~450,000 new patients are diagnosed each year. Treatment depends on the type, stage and grade of the breast cancer [50]. Early detection of tumours through X-ray mammography screening has led to a significant increase in survival rates, as well as more conservative treatments and improved cosmetic outcomes. Nevertheless, mammography has a high-rate of false-positives and further biopsy diagnosis by histopathology is required (70–90% of biopsies are found to be for benign lesion) [51]. Therefore, new alternative techniques for in-vivo diagnosis are required.

Early work by Haka et al. showed that Raman spectroscopy can discriminate between breast malignancies and healthy breast tissue [52]. Kneipp et al. used multivariate spectral analysis to discriminate between normal duct epithelia and epithelium-derived breast tumours [53]. More recently, Kong et al. used Raman micro-spectroscopy to compare spectra obtained from ductal carcinoma (DC), surrounding inflammatory stroma and tissue areas containing other components of healthy breast tissue (lobules, ducts, stroma, fat) [10]. The authors showed that the Raman spectra of DC have more intense spectral bands assigned to nucleic acids (788 cm^{-1}, 1098 cm^{-1}) compared to other tissue structures. The Raman spectra of tumour-surrounding inflammatory stroma had lower intensity bands corresponding to collagen and higher intensity bands assigned to nucleic acids compared to the Raman spectra of normal stroma.
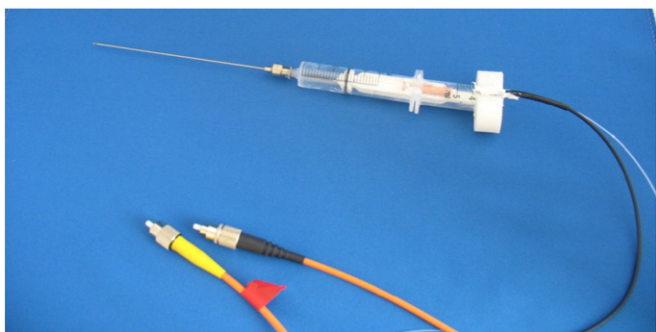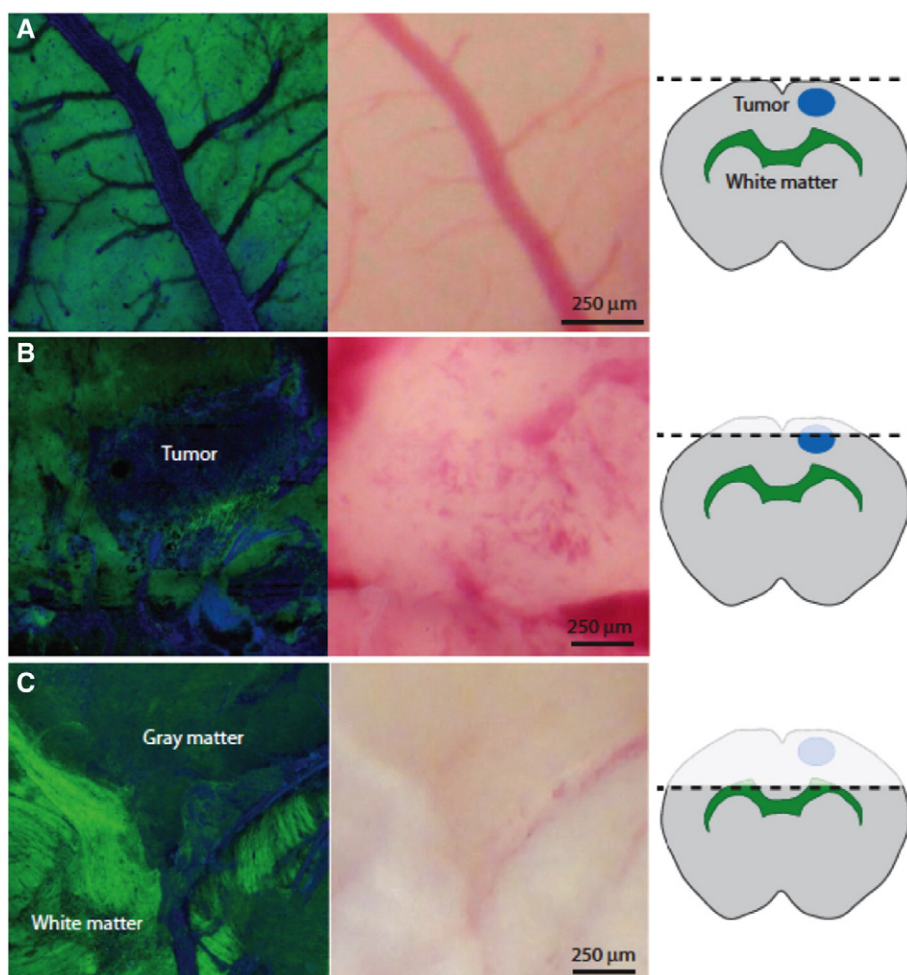
Fig. 2. Using stimulated Raman spectroscopy for in-vivo imaging mouse brain during tumour excision [49]. (A) Tumour located beneath the cortical surface; (B) the tumour is detected after removal of part of the cortex; (C) tumour was resected deep and the resection margins appear tumour-free. Reprinted with permission from Science.

Stone et al. investigated the potential for in-vivo diagnosis using TRS [54]. The main aim of the study was to measure the composition of breast calcifications and provide diagnosis for the lesions containing them — calcium oxalate is found only in benign lesions and calcium hydroxyapatite found in proliferative lesions, which include benign and malignant lesions. These preliminary studies carried out on breast phantoms showed the potential to identify calcium hydroxyapatite and calcium oxalate monohydrate from depths of up to 2–3 cm (Fig. 3). The approach of using in-vivo TRS to link the composition of breast calcification with the pathology would improve the efficiency of breast cancer screening and avoid unnecessary biopsies. A parallel study on 235 calcifications from 110 patients demonstrated the significant negative correlation between carbonate concentration and advancing malignant pathology grade [55]. TRS has been shown to provide a prediction of carbonate concentration in calcium hydroxyapatite from measuring the phosphate 960 cm^{-1} peak alone [56].

Raman spectroscopy has also been proposed for detection of tumour margins during breast cancer surgery, both in-vivo and ex-vivo. A hand-held Raman probe was developed for in-vivo collection of single-point Raman spectra during surgery [57]. The authors measured 30 Raman spectra from nine patients: 29 from margins subsequently found to be negative on pathology examination (21 were composed of normal breast tissue whereas 8 contained fibrocystic change) and 1 spectrum from a margin subsequently found to be positive on pathology examination (high-grade ductal carcinoma in-situ). Although only one malignant sample was included, this study showed the potential for in-vivo detection of tumour margins during surgery. Alternatively, confirming

negative resection margins can be achieved by analysing the surface of the resection specimen ex-vivo. To avoid sampling errors due to single point measurements, CARS has been used to provide molecular images of breast tissue and identify the tumour margins and differentiate its subtypes [58]. The authors were able to image ex-vivo human normal breast tissue, benign proliferative, as well as in-situ and invasive carcinomas. By analysing the morphological features (geometry and distribution of cancer cell nuclei) in the CARS images (typically 120 μm × 120 μm), cancerous lesions were separated from normal tissue and benign proliferative lesion: 80% of intermediate-grade invasive ductal carcinoma (IDC) and 85% of high-grade IDC were correctly distinguished [58]. A recent study based on selective-sampling Raman microscopy using integrated auto-fluorescence imaging and Raman spectroscopy demonstrated the feasibility to detect mammary carcinomas ex-vivo within time-scales compatible with intra-operative use for breast conserving [10]. In this technique, Raman spectra in the fingerprint region (600–1800 cm^{-1}) were collected at the locations indicated by the auto-fluorescence images. Objective diagnosis of mammary ductal carcinoma was achieved with only 250–550 Raman spectra for 5 mm × 5 mm tissue specimens (equivalent to ~15 min) [10].

In addition to the assessment of resection margins, the feasibility of using Raman spectroscopy for intra-operative assessment of sentinel axillary lymph nodes during breast cancer surgery has also been explored [59]. Horsnell et al. demonstrated the ability to discriminate normal and metastatic lymph nodes using multivariate classification models, achieving 85–92% sensitivity and 88–100% specificity in a leave-one-out cross-validation [60].
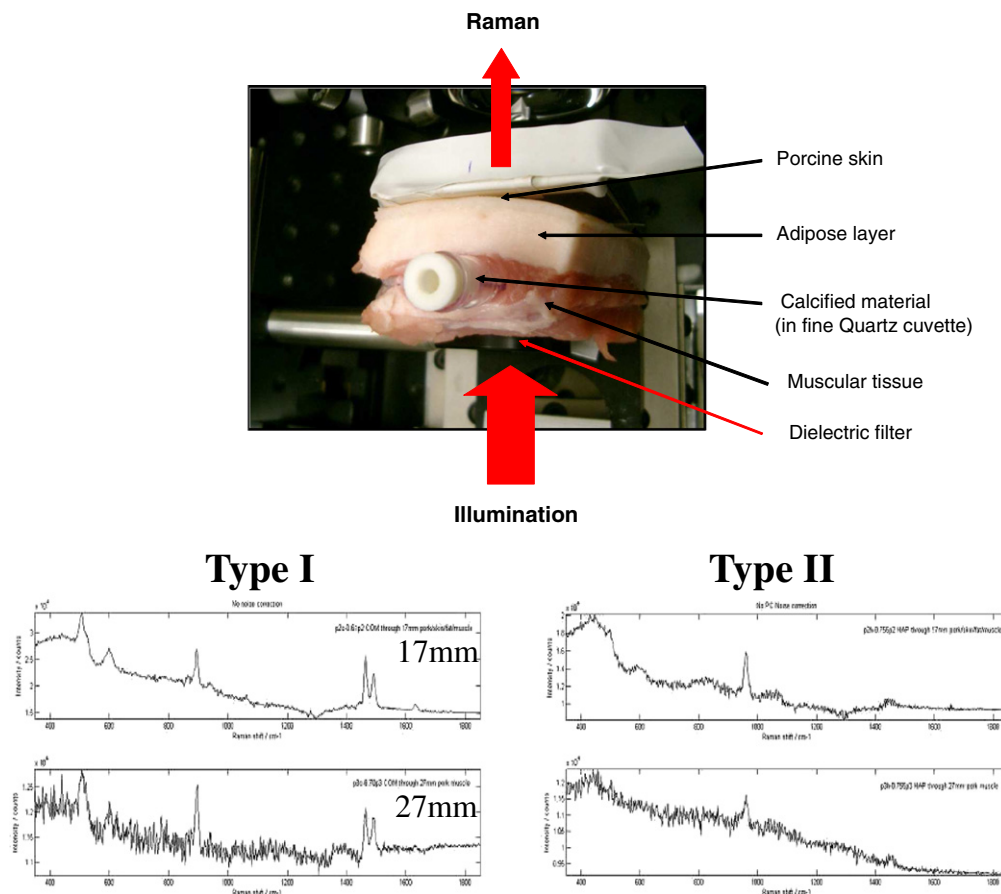
Raman

- Porcine skin
- Adipose layer
- Calcified material (in fine Quartz cuvette)
- Muscular tissue
- Dielectric filter

Illumination

Type I   Type II

17mm

27mm

Fig. 3. Experimental configuration of TRS demonstration [44] using a pork tissue block to simulate human breast and known calcification standards inserted into the centre of the tissue. 830 nm laser illumination was used. Note the clear differences in spectra measured from type I and type II calcifications. Reprinted with permission from Cancer Research.

3.3. Lung cancer

Lung cancer is the second most common cancer in humans and, despite advances in surgical, radiotherapeutic, and chemotherapeutic treatments, long-term survival rate remains low (5% at 10 years for non-small cell lung cancers) [61]. One of the main reasons for the low survival-rates is that ~75% of patients have late-stage disease, when effective treatment is unlikely to succeed. The feasibility of screening for high-risk populations is currently debated in Europe and the USA [62]. One of the major challenges for the CT screening programmes is related to the high-rate of false positives, which highlights the need for improved diagnostic techniques.

An early study conducted by Huang et al. [63] used Raman spectroscopy to distinguish tumour from normal bronchial tissue specimens, squamous cell carcinoma and adenocarcinoma. The Raman spectra of malignant tumour tissue was characterised by higher intensity bands corresponding to nucleic acids, tryptophan and phenylalanine and lower signals for phospholipids, proline and valine, compared to normal tissue. The authors found that the ratio of the Raman band intensity at 1445 cm^{-1} and 1655 cm^{-1} had high discrimination power between normal and tumour tissues.

Raman spectroscopy has also been used to predict the prognosis of non-small cell lung cancer patients by analysing surgically resected tissue sections [64]. Raman microscopy based on raster-scanning and multivariate statistical analysis was able to predict early postoperative cancer recurrence with a sensitivity of 73% and specificity of 74%. The analysis of the Raman spectra indicated that high porphyrin levels in the normal samples and intense bands corresponding to DNA in the tumour samples allowed discrimination between normal and tumour tissue. The use of CARS to provide differential diagnosis of lung-

carcinoma (adenocarcinoma, small cell carcinoma and squamous cell carcinoma) was also investigated [65]. CARS images corresponding to the CH$_2$ vibrational mode (2845 cm^{-1}) were analysed using pattern recognition algorithms and indicated significant morphological differences between normal tissue and tumour regions: cancer regions showed higher density of cells compared to normal regions, and the size and configuration of the cells corresponded with defined parameters [66].

The feasibility of increasing the diagnosis specificity for pre-neoplastic lesions in-vivo was investigated by integrating Raman spectroscopy measurements to a bronchoscope based on white light and auto-fluorescence [67]. White light and auto-fluorescence images allowed identification of suspicious lesions, areas from which Raman spectra were measured with acquisition times of 1 s. The authors showed that sensitivity of 96% and a specificity of 91% for discrimination of pre-neoplastic lesions (leave-one-out cross validations) by developing multivariate statistical models.

3.4. Skin cancer

Skin cancer is the most common type of cancer in humans. In the UK and USA more than 100,000 and 1,000,000 cases, respectively, are diagnosed annually [68,69]. Given the easy optical access to skin, numerous studies have investigating the use of Raman spectroscopy for in-vivo diagnosis of skin cancers. Preliminary work by Lieber et al. using a fibre-optic Raman probe indicated high-diagnosis accuracy for non-melanoma skin cancers: 100% sensitivity and 91% specificity for discriminating tumours from normal skin [70]. More recently, Lui et al. developed a hand-help Raman probe that allowed real-time (less than 1 s) in-vivo diagnostic [71]. Using this probe in a study on more than 1000 cases of skin cancers and other skin diseases, the authors showed
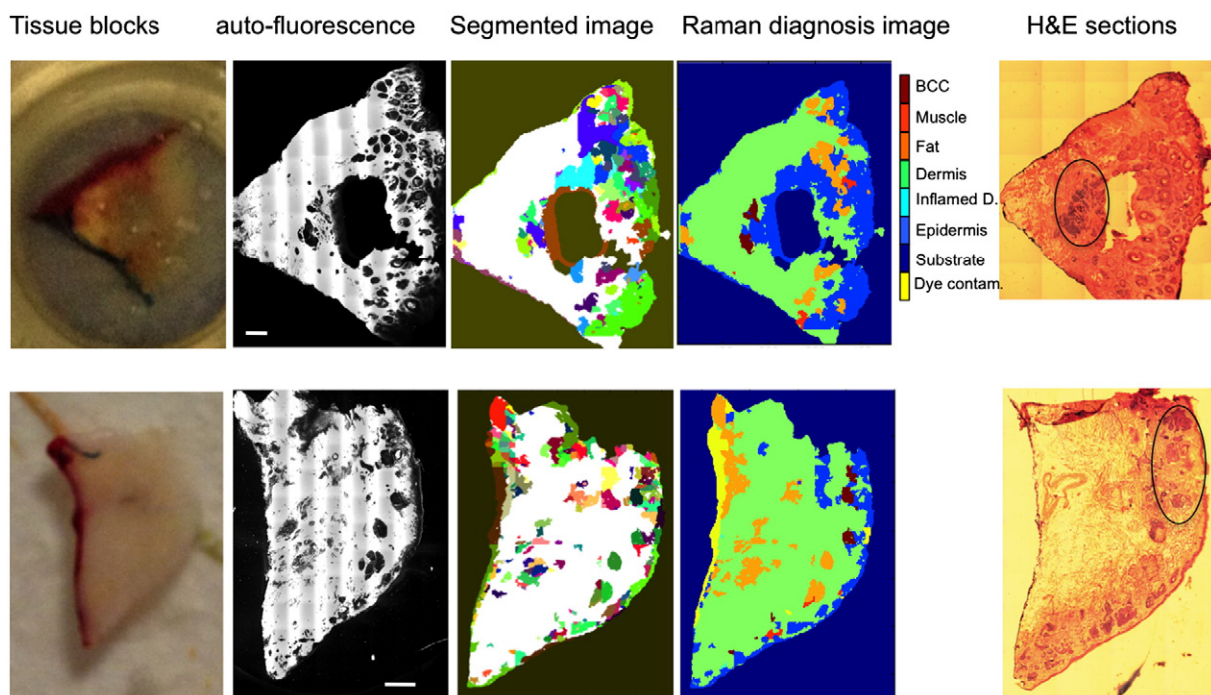
Fig. 4. Diagnosis of basal cell carcinoma of the skin (BCC) by multimodal spectral imaging based on auto-fluorescence imaging and Raman spectroscopy. Scale bar: 2 mm [7]. Reprinted with permission from the National Academy of Sciences of the United Stated of America.

that it is possible to distinguish malignant and premalignant from benign lesions, melanomas from benign pigmented skin lesions, and melanomas from seborrheic keratoses, with sensitivities between 95% and 99% [59]. Nevertheless, the specificity of these models was low, ranging between 15% and 54%, when discriminating malignant melanoma from non-melanoma pigmented lesions and seborrheic keratosis [71].

For high-risk BCCs, Mohs micrographic surgery (MMS) is the best treatment option. In this technique sequential layers of skin tissue are excised and the entire resection margin is assessed intra-operatively by frozen-section histopathology. This procedure ensures complete removal of tumour cells, while sparing as much healthy tissue as possible. The 5-year recurrence rate for BCC treated by MMS is 1.4–2.5%, significantly lower than 3.2–10% for standard excision [72]. Nevertheless, the high costs associated with intra-operative assessment of tissue resections by frozen section histopathology have limited the widespread implementation of MMS. Early studies by Nijssen et al. showed that BCC can be discriminated from normal tissue based on a higher intensity of Raman bands associated with nucleic acids [73]. A two-step classification model achieving 100% sensitivity and 93% specificity (leave-one-out cross-validation) was developed to diagnose BCC based on Raman spectra obtained by raster-scanning over areas of 0.005–0.4 mm^2 [73]. Larraona-Puy et al. reported a classification model based on selected Raman bands characteristic to nucleic acids and proteins that allows discrimination of BCC from normal tissue with 90 ± 9% sensitivity and 85 ± 9% specificity [8]. This multivariate classification model was then applied to tissue sections from new patients and obtained objective diagnosis images that agreed with histopathology. To increase the speed of diagnosis, a multimodal approach based on CARS, second-harmonic generation (SHG) and two-photon excited fluorescence (TPEF) has been recently developed elsewhere [74]. The application of CARS/TPEF/SHG multimodal microscopy allows for a characterisation of the architecture and biochemical composition, i.e., the morphochemistry of frozen section biopsy specimens. In doing so a rapid discrimination between healthy and dysplastic/tumourous tissue comparable with the gold-standard histopathology can be obtained [74,75]. Algorithms were developed to facilitate handling and interpretation of the multimodal

images to create large spectral maps that provided tissue classification and objective tumour diagnosis [48,76].

In a different multimodal approach, auto-fluorescence (AF) imaging was used to determine the main spatial features of skin resections with high spatial resolution, then this information was used in an automated manner to select and prioritise the sampling points for Raman spectroscopy. For skin samples of 4 mm × 4 mm, the AF-Raman multimodal approach provided diagnosis similar to raster scanning Raman microscopy but with a dramatic increase in acquisition speed: AF-RS typically required ~100-fold fewer Raman spectra compared to raster scanning [7]. Fig. 4 shows typical examples of using AF-Raman for detection of BCC in skin resections obtained during Mohs surgery. Accurate assessment of resection margins was obtained with only 500–1500 Raman spectra for skin samples of 1 × 1 cm^2 removed during Mohs surgery, without requiring sectioning, staining or any other tissue preparation stage [7].

3.5. Oesophagus

In response to the twin stimuli of the need for improved surveillance and targeted endotherapies, a number of emerging technologies are being developed with the aim of improving the identification of Barrett's oesophagus and associated neoplasia. The ability of Raman spectroscopy to discriminate between 8 pathological groups from normal squamous through to cancer has been demonstrated. A biopsy targeting model, differentiating normal vs. Barrett's vs. dysplasia/adenocarcinoma, achieved a high level of agreement with consensus pathological opinion [77]. Much work in the oesophagus has been aimed at the development of a fibre-optic Raman probe for in vivo use, designed to be compatible with medical endoscopes. Initial work in rat models in-vitro showed potential for in vivo applications [78]. Safety and feasibility of using Raman probes in the oesophagus were shown using an Enviva Visionex probe. 400 spectra in 20 patients were measured using 5 second acquisition times, although discrimination of pathology was poor [79] due to large sampling depths. This was followed up with a custom-built probe which was used to discriminate Barrett's, low-grade dysplasia (LGD) and high-grade dysplasia

(HGD)/adenocarcinoma with accuracy 88%, 81% and 92% respectively in 192 spectra from 65 patients with Barrett's oesophagus using 5 second acquisition times [80].

In vivo diagnosis of oesophageal cancer with Raman fibre-optic probes has been reported with sensitivity 91% and specificity 94%, although subtypes of cancer or degrees of dysplastic change were not differentiated. This study measured 263 oesophageal Raman spectra from 80 patients (33 with cancer) with relatively fast acquisition times of 0.4–0.5 s [81,82]. Accurate recognition of pathology subtypes using spectra acquired in 1 s using a Raman probe, giving sensitivities and specificities for normal squamous of 87% and 96% respectively, Barrett's/LGD 72% and 91%, HGD/ adenocarcinoma 86% and 88%. Using a 2 group model with spectra acquired over 5 s the detection rate of HGD/ adenocarcinoma remained 86%, but the specificity was greatly improved at 98% [83].

Raman spectral mapping of oesophageal tissue micro-sections has been used to characterise the biochemical changes underlying the spectral differences. Pseudo-colour principal component score maps were used identify altered cellular constituents associated with malignancy. Dysplastic glandular tissue showed higher levels of DNA, actin and oleic acid, whereas normal squamous tissue had a higher glycogen content [84]. Rapid mapping of tissue sections using Raman spectroscopy has the potential to be used as an automated histopathology tool. Hutchings et al. showed that mapping could be performed in clinically applicable timescales e.g. 2 mm diameter sections over 30–90 min, and that this was sufficient to discriminate pathology [3,85].

3.6. Prostate cancer

Prostate cancer is one of the most cancer types in men, accounting for approximately a quarter of all new cancer cases. Crow et al. were the first to describe the use of Raman spectroscopy in prostatic disorders [86]. Raman spectra obtained from the prostate suggested that the variations in the glycogen and nucleic acid content between benign prostatic hypertrophy (BPH) and adenocarcinoma [86]. As Raman spectroscopy examines tissue at the molecular level, it has the potential to provide additional prognostic information in early prostate cancer. Raman spectroscopy can be used in determining the biochemical basis for the different pathologies within the prostate gland [87]. Further, the authors suggested that the potential in-vivo applications of the technique could be for guiding prostate biopsy procedures and the intra-operative assessment of tumour resection margins during radical prostatectomy. In vitro, Raman spectroscopy can be used to accurately identify BPH and three different grades of prostatic adenocarcinoma. The prostate algorithm was able to differentiate benign samples (benign prostatic hyperplasia and prostatitis) from prostate cancer, with an overall accuracy of 86%. As Raman probes are suitable for use during endoscopic, laparoscopic, or open procedures, this work paves the way for in vivo studies [88].

Raman spectra were measured from two well-differentiated, androgen-sensitive cell lines and two poorly differentiated, androgen-insensitive cell lines to differentiate between carcinoma prostate cell lines of varying degrees of biological aggressiveness. Crow et al. were able to identify the individual cell lines with an overall sensitivity of 98% and a specificity of 99% and demonstrated promising results of Raman spectroscopy in the diagnosis and grading of carcinoma of the prostate [89]. Grubisha et al. demonstrated the low-level and simultaneous determination of many complexed forms of prostate specific antigen (PSA) using surface-enhanced Raman scattering (SERS) [90].

A recent review summarises clinical applications of the various Raman technologies available for prostate cancer diagnosis [91].

3.7. Colorectal cancer

Early identification and eradication of tumours is critical for improving the treatment outcome for patients with colorectal cancer. Although screening by colonoscopy has significantly increased the survival rates

for patients, this technique has low specificity for discrimination of adenoma and early adenocarcinomas from benign hyperplastic polyps in-vivo. Other reviews have detailed the application of optical techniques to colon cancer [92,93]. Initial studies using near-infrared Raman spectroscopy investigated in vitro differentiation of normal mucosa, metaplastic and adenomatous polyps and adenocarcinomas, achieving sensitivities and specificities greater than 90% when compared with conventional histopathology [38,79]. In the first in-vivo study using 'Visionex' Enviva fibre-optic Raman probes, the probe passed down the accessory channel of a conventional colonoscope showed the ability to differentiate between normal colon and hyperplastic and adenomatous polyps with a sensitivity of 100%, specificity of 89% and overall accuracy of 95% with spectra measured from 19 regions of 9 polyps in 3 patients [94]. Elsewhere, an in-house developed Raman probe for ex-vivo measurements on 105 colon specimens from either biopsies or partial colectomies (41 normal specimens, 18 hyperplastic polyps and 46 adeno-carcinomas) from 59 patients. Diagnostic accuracy was in excess of 98%. This study did not include adenomas, which are an intermediate pathological group in the stepwise progression from normal tissue to adenocarcinomas. With acquisition times of 5 s, the authors developed diagnostic algorithms that identified normal tissue with 98.8–99.8% sensitivity 100% specificity, hyperplastic polyps with 100% sensitivity and 100% specificity, and cancerous tissue with 100% sensitivity and 98.1–99.7% specificity [95].

A confocal endoscopic two-fibre-optic probe [35] was utilised on ex-vivo colonic tissues to evaluate its potential in vivo performance. Biopsies were collected and snap frozen, then measured with the probe applied to the epithelial surface once defrosted. A miniature Raman-endoscope system was used to measure spectra sequentially over a period of several weeks to monitor tumour progression in 4 mice with recognisable tumour lesions. Molecular changes in the tumour as it progressed, such as altered collagen type I and lipid content were measured and they were able to classify 86.8% of samples correctly as tumour versus normal tissue, when compared to histopathology [96].

Recent work by Short et al. has examined the possible use of high frequency Raman spectroscopy in the colon, measuring wavenumbers in the range 2050 to 3100 cm^{-1} [97]. Although discriminatory peaks were mostly detected at lower wavenumbers, measuring in this higher range reduces the effects of tissue auto-fluorescence and emissions in the fibre-optic probe itself. This means that cheaper probes can be produced without the need to filter the light within the probe. This small study in ex vivo fresh tissue samples has shown that discrimination of pathology subtypes is possible using these higher wavenumbers with 1 second acquisition times.

Raman spectroscopy has also been investigated as a potential adjunct to histopathology, with the ultimate aim of either automated sample analysis, or digital staining of a tissue section to assist pathologist analysis. Rapid Raman mapping of snap-frozen tissue sections used in conjunction with chemometric analytical techniques to interpret spectral information, and demonstrated the ability to identify many subtle histological features of colonic polyps. This technique thus has the potential to reveal more biochemical information about a tissue sample than standard chemical staining [98].

3.8. Bone disease

Many bone diseases arise because of subtle changes in the bone protein chemistry but these are invisible to conventional techniques like X-rays. Raman spectroscopy is potentially able to detect these subtle molecular changes and its potential to enhance the diagnosis of osteoarthritis (OA), brittle bone disease and fragility fractures has been investigated. Frequency shifts serve as an important source of contrast in assessing tissue composition such as carbonate substitutions for phosphate positions in bone. The extracellular matrix also provides another source of contrast to bone tissue composition. The extracellular matrix contains many protein-rich vibrational modes, corresponding
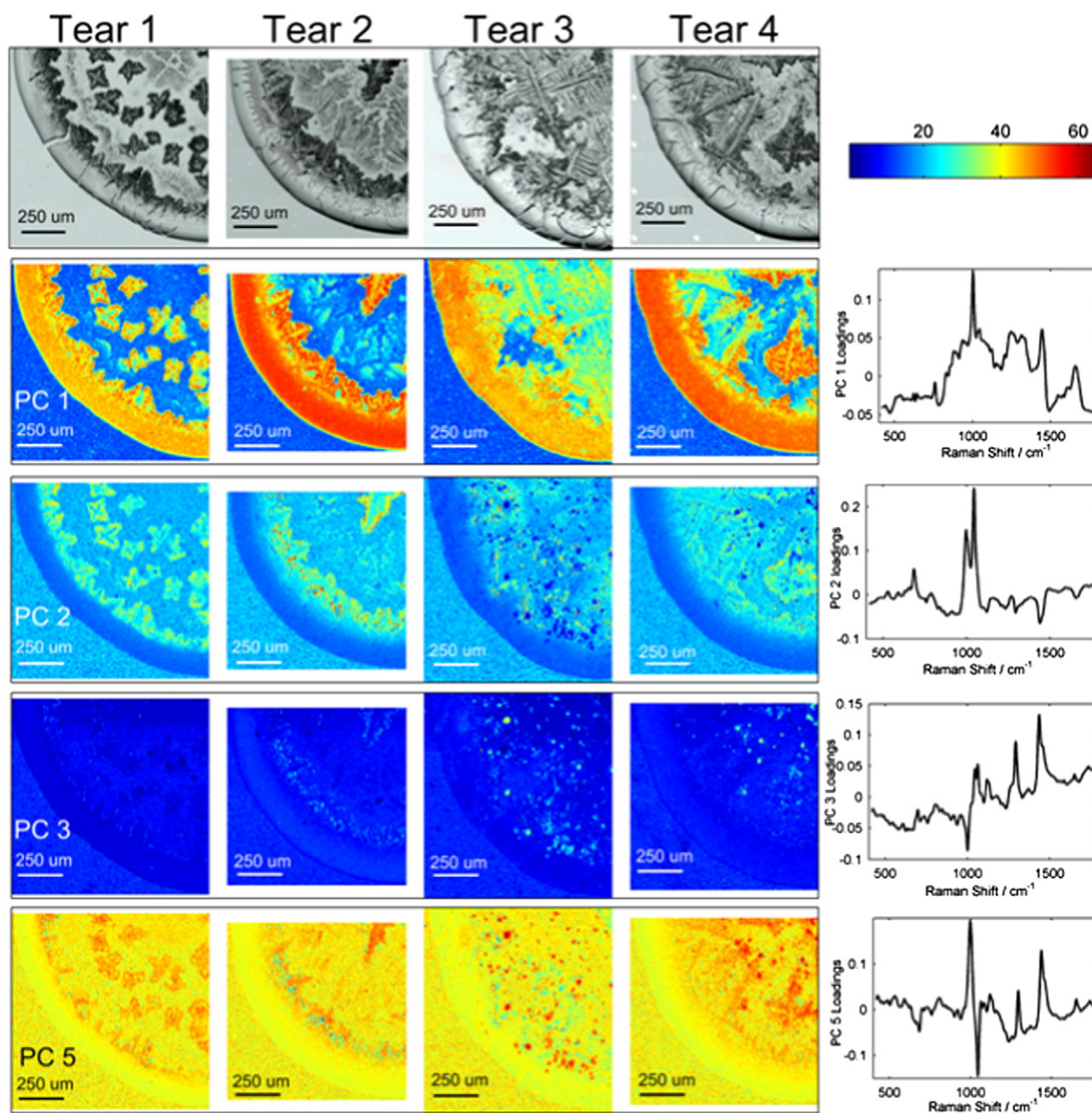
Fig. 5. Four human tear samples drop dried on calcium fluoride substrates and measured with 830 nm Raman microscopy. Top row white light images, subsequent rows are PC score maps and associated loadings (far right). All images are displayed on the same scale [106]. Reprinted with permission from Science Driect.

predominantly to collagen features such as amide backbone, protein secondary structure, and side chain composition.

Early studies compared the Raman spectral features of bone with those of their major components, such as hydroxy and carbonated apatite [99]. Raman spectroscopy has been used to evaluate alterations to bone composition associated with ageing, disease, or injury to aid in the diagnosis and prediction of fragility fractures [100]. OA is a common debilitating disease that results in degeneration of cartilage and bone in the synovial joints. Raman spectroscopy has shown that subtle changes in the molecular structure of the subchondral bone matrix, or inherent differences, exist in both the medial and lateral (beneath intact cartilage) compartments of OA knees [101].

SORS enables the chemistry of bone tissue to be safely determined several millimetres beneath the skin [102]. In-vivo SORS measurements have been carried out investigating the potential for the detection of OA [103]. Improvements in the quality of in vivo Raman spectra can be obtained using the inverse SORS approach [26], as greater laser powers can be applied for the same total laser intensity.

4. Biofluid diagnostic assays based on Raman spectroscopy

The analysis of biofluids, such as blood and urine, can enable powerful minimally invasive diagnostics for many diseases [104]. Biofluid assays have several key advantages (accessibility, require less invasive procedure, allow repeated sampling) and biofluid diagnostic can be implemented in a variety of healthcare scenarios, from being part of routine health checks to intra-operative monitoring of blood or therapeutic agents.

Bodily fluids can contain numerous biomolecules of diagnostic interest, although not always of sufficient concentration to be measured in solution with Raman spectroscopy. One highly affective approach to pre-concentrate the proteins found in the fluids is drop coated deposition Raman spectroscopy (DCDRS) (Fig. 5). This has been shown to provide an accurate measure of the concentration of protein mixtures in solutions even when pre-concentrated [105]. The use of DCDRS has been demonstrated in human tears indicating promise for measurement of both local and systemic disease biomarkers [106,107].

4.1. Diabetes and glucose level monitoring

For diabetes patients, the blood glucose levels must be monitored on a regular basis, in some cases as often as four or five times a day. Nevertheless, the current devices used for measuring blood glucose level rely on invasive procedures to produce a blood sample for analysis (e.g. requiring pricking), which are painful and inconvenient for patients.

Raman spectroscopy has been used to measure the concentrations of chemicals in blood serum (glucose, urea, proteins, cholesterol, triglycerides, etc.), with results in good correlation with reference values [108, 109]. Studies carried out on mouse blood samples showed that the Raman band characteristic to glucose at 1125 cm^{-1} can be used to measure the concentration of glucose in the blood [109]. In-vivo measurements performed transcutaneously (blood vessel in the mouse ear) showed a linear correlation coefficient of 0.91 between the glucose concentration recorded by Raman spectroscopy and reference values obtained by a blood glucose metre. To increase the sensitivity required for rapid glucose detection at the physiological concentrations' clinically relevant range (0.56–25 mM), enhancement of the Raman signals by SERS has been proposed [110]. SERS substrates based on functionalised silver coated self-assembled polystyrene nanospheres were used to measure in-vitro glucose levels within the physiological range with a root mean squared error of prediction of 4.62 mM [111]. Similar SERS substrates were implanted in mice and the feasibility of in-vivo monitoring glucose levels by transcutaneous SESORS measurements was demonstrated [112].

A recent study employed Raman spectroscopy for diagnostic of type II diabetes by detecting molecular changes in the membranes of erythrocytes [113]. The membrane of red blood cells in patients with type II diabetes is continuously exposed to high blood glucose levels, leading to damage in structural components. Correlation between membrane damage and glucose levels has been established by high-performance liquid chromatography and thin-layer chromatography, but these techniques require laborious procedures [114]. Raman spectroscopy measurements in the high-wavenumber region showed that lipid damages (decreased liquidity, altered phospholipid organisation) in diabetic erythrocytes and multivariate statistical method achieved a diagnostic accuracy of 98.8% for differentiating diabetic versus normal erythrocytes.

4.2. Cancer diagnostics

Detection of genetic and epigenetic materials originating from tumour or circulating tumour cells in body fluids represents an attractive alternative for faster and non-invasive detection of early cancers.

The feasibility of analysing urine samples by Raman spectroscopy aimed at detection of prostate cancer cells was first investigated by Harvey et al. [115]. Integrated Raman microscopy and optical tweezers was used to discriminate between malignant cells and bladder cells, given the likelihood that both cell types will be present in urine samples. The Raman spectra of the two cell types suggested a higher concentration of nucleic acids and proteins in the bladder cells compared to the prostate cancer cells. Further work included androgen sensitive CaP cell-line LNCaP, primary benign prostate hyperplasia cells and primary urethral cells [116]. Multivariate classification models based on principal component-linear discriminate analysis indicated sensitivities and specificities of >93% and 98% respectively, using a validation test based on blind comparison.

A proof-of-concept study was reported by Taleb et al. [117] that used Raman spectroscopy to analyse blood serum to discriminate cirrhotic patients with and without hepatocellular carcinoma. Hepatocellular carcinoma represents ~90% of primary liver cancers and is the third most common cancer death worldwide. Rapid and easy-to-use diagnostic tools are required to allow detection of tumours at early stages when patients are eligible for curative treatments. Multivariate spectral analysis models were developed achieving an overall rate of accuracy

of ~86–91%. Similar proof-of-principle studies based on blood serum analysis by Raman spectroscopy have also been carried out for early diagnostic of breast [118] and head-and-neck cancers [119].

Raman spectroscopy has been extensively used for analysis of white blood cells as a potential diagnostic tool for lymphomas and leukaemia. Early work by Chan et al. showed that single-cell Raman microspectroscopy was able to discriminate between normal human lymphocytes and transformed Jurkat and Raji lymphocyte cell lines based on highly reproducible biomolecular fingerprints [120]. The neoplastic cells were found to have lower DNA bands (785 cm^{-1}, 1098 cm^{-1}) but stronger band characteristic to proteins (1126 cm^{-1}, 1447 cm^{-1}) compared to normal lymphocytes. Multivariate statistical models based on Raman spectra achieved a sensitivity of 98.3% for cancer detection, with 97.2% of the cells being correctly classified as belonging to the normal or transformed type. The same research group found similar high diagnostic accuracy for normal T and B lymphocytes from healthy individuals and cells from leukaemia patients, based on Raman spectra of individual cells [121].

Apart from confocal Raman microscopy, SERS has also been proposed for phenotypic identification of white blood cells aimed at developing diagnostic tools for haematological malignancies [122]. Antibody-targeted, PEG-coated gold nanoparticles were used simultaneously to label three cell surface markers of interest on malignant B cells from the LY10 lymphoma cell line. The authors demonstrated the high specificity of these SERS particles on primary chronic lymphocytic leukaemia and LY10 cells.

Non-invasive prostate cancer screening methods using serum surface-enhanced Raman scattering (SERS) have been carried out using serum samples from 93 prostate cancer patients and 68 healthy volunteers by silver nanoparticles. Three types of kernel functions including linear, polynomial, and Gaussian radial basis function (RBF) were employed to build support vector machine (SVM) diagnostic models for classifying measured SERS spectra. The study showed that for the RBF kernel SVM diagnostic model achieved a diagnostic accuracy of 98.1%, demonstrating that label-free serum SERS analysis technique is a promising tool for non-invasive prostate cancer screening [123].

The feasibility of detecting circulating tumour cells in the blood by Raman spectroscopy has been recently investigated using integrated Raman spectroscopy and optical tweezers based on microfluidic chips. These integrated instruments allowed measurements of Raman spectra of individual blood cells and were able to detect spectral features characteristic to tumour cells [124,125]. The performance of this system was tested for a tumour cell model that consisted of leucocytes extracted from blood, breast cancer cells BT-20 and MCF-7 and leukaemia cells OCI-AML3. A multivariate spectral model was developed that allowed classification of the cells with sensitivities between 97 and 100% (determined by iterated 10-fold cross-validation) [124].

4.3. Asthma

Assignment of asthma patients to a correct category (mild, moderate, severe or very severe) is important to allow the selection of an optimal treatment. An assay based on Raman spectroscopy analysis of blood serum was proposed for diagnosing asthma and monitoring treatment response [126]. The assay was carried out on serum samples from 44 asthma patients of different grades (mild, moderate, treated severe and untreated severe) and from 15 reference subjects. The results showed that changes in protein structure and increase in Raman bands characteristic to DNA and glycosaminoglycans were linked with increase in asthma severity.

4.4. Inflammatory response

Raman spectroscopy was proposed to measure and quantify the concentration of C-reactive protein (CRP) in blood plasma [127]. CRP is a protein that can be used as a sensitive biomarker of inflammation

and is often used to detect bacterial infection because it is less sensitive to viral infections. The typical concentration of CRP in humans is less than 10 mg/l, and can increase 2–3 orders of magnitude during inflammation. The concentration of CRP is typically measured using immunoassays that rely on laborious, expensive and time-consuming procedures. Berholt et al. showed that a multivariate model based on partial least square analysis (samples obtained from 40 patients) allowed quantification of CRP in blood serum with a root mean square error of cross-validation of 10.8 mg/l [127].

Raman spectroscopy was used to establish reliable biomarkers that can be used to distinguish between non-infectious systemic inflammatory response syndrome (SIRS) and sepsis [128]. The study was based on Raman spectral measurements of blood samples obtained from 31 patients with sepsis and 39 patients classified with SIRS without infection. A multivariate analysis model was developed that achieved a prediction accuracy of 80% on an independent dataset.

4.5. Coagulant and anti-coagulant factors in human blood

Multivariate analysis based on partial least square regressions was also used to measure the concentration of fibrinogen concentration in blood plasma [129]. Fibrinogen is a glycoprotein present in the human blood that helps coagulation (normal level of fibrinogen in the blood is 1.5–3 g/l). The activation of fibrinogen is involved in the pathogenesis of inflammation, tumour growth and various diseases (concentrations 4–8 g/l). This preliminary study carried out on blood samples from 34 patients achieved a root mean square error of prediction of 0.72 ± 0.05 g/l. While the accuracy of Raman spectroscopy was lower than the gold-standard assay (Clauss fibrinogen assay for measuring thrombin clotting time), Raman spectroscopy is an attractive technique as it can provide rapid and reagent-free quantitative results.

The use of Raman spectroscopy for monitoring the amount of heparin in patients' blood during surgery has also been investigated [130]. Calibration models based on partial least squares were able to detect low concentrations of heparin in serum (~8 USP/ml) with a root mean square error of prediction ~4 USP/ml.

4.6. Malaria

Malaria is one of the most deadly diseases of humans, responsible for more than 1 million deaths in 2010 [131]. Early diagnosis of malaria is important for decreasing mortality rates and reducing the overuse of antimalarial drugs.

Raman spectroscopy has been extensively used for studying red blood cells, including comparison between healthy erythrocytes and erythrocytes infected with the malaria parasite *Plasmodium falciparum* [132,133]. Given the strong signals due to the resonant Raman scattering, the spatial distribution of haemoglobin and hemozoin was analysed within individual blood cells.

In addition to analysing the red blood cells, recent studies have focused on the analysis of blood plasma, as potentially a more efficient diagnostic method compared to blood smears. In malaria infected patients, rupture of erythrocytes releases hemozoin, heme and parasites into the blood stream, which can be detected by Raman spectroscopy analysis of plasma or serum in a more efficient way than current tests based on microscopic evaluation of blood smears. The feasibility of this approach has been investigated by Hobro et al. [134]. Raman spectroscopy was used to monitor the changes in plasma during *Plasmodium* infection in mice, following malaria disease progression over the course of 7 days (Fig. 6). The Raman bands corresponding to haemoglobin and hemozoin indicated changes in the very early stages of infection, as early as one day after *Plasmodium* infection. On the other hand, changes in membranes of erythrocyte were detected only around day 4, indicating that plasma-based Raman assay may be more advantageous for detection of malaria.
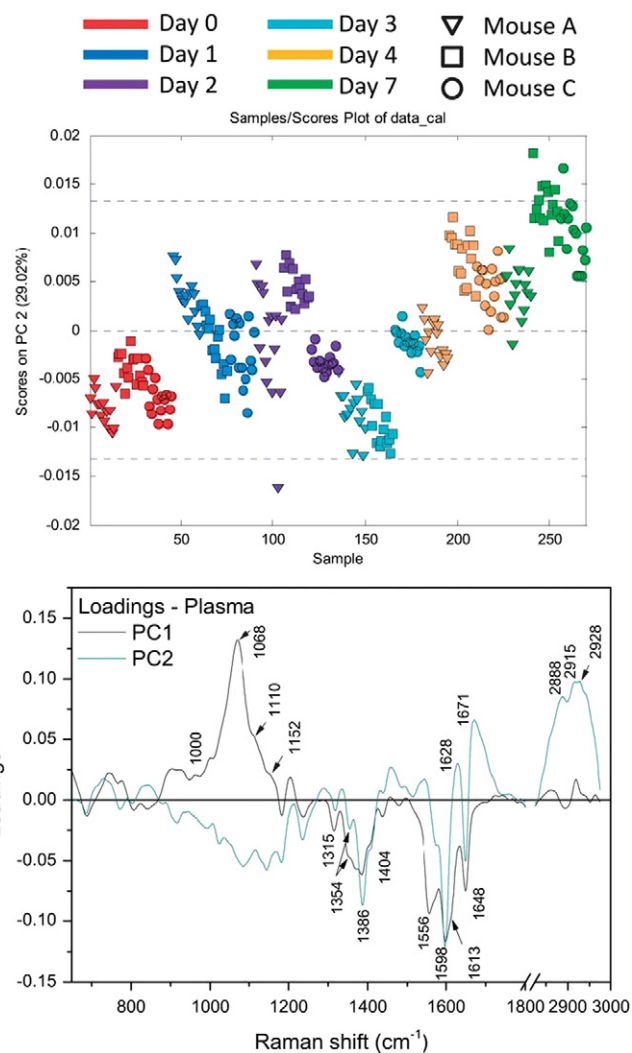

Fig. 6. Principal component analysis of Raman spectra measured for blood plasma from *Plasmodium* infected mice. Samples are as follows: day 0 (red), day 1 (dark blue), day 2 (purple), day 3 (light blue), day 4 (orange) and day 7 (green). Mice A are shown as triangles, mice B as squares and mice C as circles [134]. Reprint with permission from the Royal Society of Chemistry.

5. Conclusions

The broad range of techniques and applications presented in this article demonstrate the potential of Raman spectroscopy for medical diagnostics, as well as the high interest in this technique. Raman spectroscopy can achieve high diagnosis accuracy, and results in many applications that have been confirmed across numerous different laboratories. Compared to other diagnostics assays, Raman spectroscopy can be non-invasive, fast, and can achieve high chemical specificity based entirely on intrinsic molecular contrast in biological samples. In addition, most Raman spectroscopy techniques rely on established optical technologies and offer cost-effective approaches when compared to conventional medical imaging techniques, such as MRI, CT or ultrasound.

One of the most important features of Raman spectroscopy is the ability to provide quantitative molecular information that can be translated into an objective diagnosis. Many optical imaging and microscopy techniques used in medical diagnostics (including the gold standard histopathology) aim to identify diseased cells based on their distribution, morphology, or interaction with specific stains or antibodies. However, such techniques provide images that require subjective interpretation, thus are prone to high inter-observer variability. Raman

spectroscopy can measure both morphological and chemical information in samples and multivariate classification models can be developed to provide objective diagnosis of independent tissue samples obtained from new patients.

The relatively low speed of Raman spectroscopy has been a main weakness for clinical translation. However, recent advances in multimodal imaging and non-linear microscopy have demonstrated the ability to obtain high-contrast molecular images and provide objective diagnosis for samples with clinically relevant dimensions and at speeds compatible with clinical use. Important progress has also been reported in sub-surface deep Raman spectroscopy, and innovative solutions and optimised designs for fibre-optic and needle Raman probes have been reported for in-vivo diagnostic. The key challenge now is the clinical translation and adoption of Raman technologies in the healthcare service. These technologies must show improved clinical outcome based on randomised clinical trials and need to demonstrate cost-effectiveness compared to current practice.

References

[1] M. Delhaye, P. Dhamelincourt, Raman microprobe and microscope with laser excitation, J. Raman Spectrosc. 3 (1975) 33–43.

[2] C.J. de Grauw, C. Otto, J. Greve, Line-scan Raman microspectrometry for biological applications, Appl. Spectrosc. 51 (1997) 1607–1612.

[3] J. Hutchings, C. Kendall, B. Smith, N. Shepherd, H. Barr, N. Stone, The potential for histological screening using a combination of rapid Raman mapping and principal component analysis, J. Biophotonics 2 (2009) 91–103.

[4] M. Okuno, H.-o. Hamaguchi, Multifocus confocal Raman microspectroscopy for fast multimode vibrational imaging of living cells, Opt. Lett. 35 (2010) 4096–4098.

[5] L. Kong, J. Chan, A rapidly modulated multifocal detection scheme for parallel acquisition of Raman spectra from a 2-D focal array, Anal. Chem. 86 (2014) 6604–6609.

[6] S. Schlucker, M.D. Schaeberle, S.W. Huffman, I.W. Levin, Raman microspectroscopy: a comparison of point, line, and wide-field imaging methodologies, Anal. Chem. 75 (2003) 4312–4318.

[7] K. Kong, C.J. Rowlands, S. Varma, W. Perkins, I.H. Leach, A.A. Koloydenko, H.C. Williams, I. Notingher, Diagnosis of tumors during tissue-conserving surgery with integrated autofluorescence and Raman scattering microscopy, Proc. Natl. Acad. Sci. U. S. A. 110 (2013) 15189–15194.

[8] M. Larraona-Puy, A. Ghita, A. Zoladek, W. Perkins, S. Varma, I.H. Leach, A.A. Koloydenko, H. Williams, I. Notingher, Development of Raman microspectroscopy for automated detection and imaging of basal cell carcinoma, J. Biomed. Opt. 14 (2009).

[9] T. Meyer, N. Bergner, C. Bielecki, C. Krafft, D. Akimov, B.F.M. Romeike, R. Reichart, R. Kalff, B. Dietzek, J. Popp, Nonlinear microscopy, infrared, and Raman microspectroscopy for brain tumor analysis, J. Biomed. Opt. 16 (2011).

[10] K. Kong, F. Zaabar, E. Rakha, I. Ellis, A. Koloydenko, I. Notingher, Towards intra-operative diagnosis of tumours during breast conserving surgery by selective-sampling Raman micro-spectroscopy, Phys. Med. Biol. 59 (2014) 6141–6152.

[11] K. Kong, C.J. Rowlands, H. Elsheikha, I. Notingher, Label-free molecular analysis of live Neospora caninum tachyzoites in host cells by selective scanning Raman micro-spectroscopy, Analyst 137 (2012) 4119–4122.

[12] K. Kong, C.J. Rowlands, S. Varma, W. Perkins, I.H. Leach, A.A. Koloydenko, A. Pitiot, H.C. Williams, I. Notingher, Increasing the speed of tumour diagnosis during surgery with selective scanning Raman microscopy, J. Mol. Struct. 1073 (2014) 58–65.

[13] S.V. Christopher, J. Rowlands, William Perkins, Iain Leach, Hywel Williams, Ioan Notingher, Rapid acquisition of Raman spectral maps through minimal sampling: applications in tissue imaging, J. Biophotonics 1 (2012) 1–10.

[14] C.L. Evans, E.O. Potma, M. Puoris'haag, D. Cote, C.P. Lin, X.S. Xie, Chemical imaging of tissue in vivo with video-rate coherent anti-Stokes Raman scattering microscopy, Proc. Natl. Acad. Sci. U. S. A. 102 (2005) 16807–16812.

[15] C.H. Camp Jr., Y.J. Lee, J.M. Heddleston, C.M. Hartshorn, A.R.H. Walker, J.N. Rich, J.D. Lathia, M.T. Cicerone, High-speed coherent Raman fingerprint imaging of biological tissues, Nat. Photonics 8 (2014) 627–634.

[16] B.G. Saar, C.W. Freudiger, J. Reichman, C.M. Stanley, G.R. Holtom, X.S. Xie, Video-rate molecular imaging in vivo with stimulated Raman scattering, Science 330 (2010) 1368–1370.

[17] M. Moskovits, Surface-enhanced spectroscopy, Rev. Mod. Phys. 57 (1985) 783–826.

[18] M. Fleischmann, P.J. Hendra, Aj McQuilla, Raman spectra of pyridine adsorbed at a silver electrode, Chem. Phys. Lett. 26 (1974) 163–166.

[19] D.L. Jeanmaire, R.P. Vanduyne, Surface Raman spectroelectrochemistry part 1. Heterocyclic, aromatic, and aliphatic-amines absorbed on anodized sliver electrode, J. Electroanal. Chem. 84 (1977) 1–20.

[20] M.G. Albrecht, J.A. Creighton, Anomalously intense Raman spectra of pyridine at a silver electrode, J. Am. Chem. Soc. 99 (1977) 5215–5217.

[21] A. Otto, I. Mrozek, H. Grabhorn, W. Akemann, Surface-enhanced Raman scattering, J. Phys. Condens. Matter 4 (1992) 1143–1212.

[22] M. Schuetz, D. Steinigeweg, M. Salehi, K. Koempe, S. Schluecker, Hydrophilically stabilized gold nanostars as SERS labels for tissue imaging of the tumor suppressor p63 by immuno-SERS microscopy, Chem. Commun. 47 (2011) 4216–4218.

[23] P. Matousek, I.P. Clark, E.R.C. Draper, M.D. Morris, A.E. Goodship, N. Everall, M. Towrie, W.F. Finney, A.W. Parker, Subsurface probing in diffusely scattering media using spatially offset Raman spectroscopy, Appl. Spectrosc. 59 (2005) 393–400.

[24] M.V. Schulmerich, K.A. Dooley, M.D. Morris, T.M. Vanasse, S.A. Goldstein, Transcutaneous fiber optic Raman spectroscopy of bone using annular illumination and a circular array of collection fibers, J. Biomed. Opt. 11 (2006).

[25] R. Baker, P. Matousek, K.L. Ronayne, A.W. Parker, K. Rogers, N. Stone, Depth profiling of calcifications in breast tissue using picosecond Kerr-gated Raman spectroscopy, Analyst 132 (2007) 48–53.

[26] P. Matousek, N. Stone, Emerging concepts in deep Raman spectroscopy of biological tissue, Analyst 134 (2009) 1058–1066.

[27] P. Matousek, N. Stone, Recent advances in the development of Raman spectroscopy for deep non-invasive medical diagnosis, J. Biophotonics 6 (2013) 7–19.

[28] P. Matousek, A.W. Parker, Bulk Raman analysis of pharmaceutical tablets, Appl. Spectrosc. 60 (2006) 1353–1357.

[29] P. Matousek, N. Stone, Prospects for the diagnosis of breast cancer by noninvasive probing of calcifications using transmission Raman spectroscopy, J. Biomed. Opt. 12 (2007).

[30] N. Stone, K. Faulds, D. Graham, P. Matousek, Prospects of deep Raman spectroscopy for noninvasive detection of conjugated surface enhanced resonance Raman scattering nanoparticles buried within 25 mm of mammalian tissue, Anal. Chem. 82 (2010) 3969–3973.

[31] N. Stone, M. Kerssens, G.R. Lloyd, K. Faulds, D. Graham, P. Matousek, Surface enhanced spatially offset Raman spectroscopic (SESORS) imaging — the next dimension, Chem. Sci. 2 (2011) 776–780.

[32] H.-n. Xie, R. Stevenson, N. Stone, A. Hernandez-Santana, K. Faulds, D. Graham, Tracking bisphosphonates through a 20 mm thick porcine tissue by using surface-enhanced spatially offset Raman spectroscopy, Angew. Chem. Int. Ed. 51 (2012) 8509–8511.

[33] K. Ma, J.M. Yuen, N.C. Shah, J.T. Walsh Jr., M.R. Glucksberg, R.P. Van Duyne, In vivo, transcutaneous glucose sensing using surface-enhanced spatially offset Raman spectroscopy: multiple rats, improved hypoglycemic accuracy, low incident power, and continuous monitoring for greater than 17 days, Anal. Chem. 83 (2011) 9146–9152.

[34] M.S. Bergholt, W. Zheng, K. Lin, K.Y. Ho, M. Teh, K.G. Yeoh, J.B.Y. So, Z. Huang, Characterizing variability in in vivo Raman spectra of different anatomical locations in the upper gastrointestinal tract toward cancer detection, J. Biomed. Opt. 16 (2011).

[35] J.C.C. Day, R. Bennett, B. Smith, C. Kendall, J. Hutchings, G.M. Meaden, C. Born, S. Yu, N. Stone, A miniature confocal Raman probe for endoscopic use, Phys. Med. Biol. 54 (2009) 7077–7087.

[36] J.C.C. Day, N. Stone, A subcutaneous Raman needle probe, Appl. Phys. Lett. 67 (2013) 349–354.

[37] Z. Huang, S.K. Teh, W. Zhen, J. Mo, K. Lin, X. Shao, K.Y. Ho, M. Teh, K.G. Yeoh, Integrated Raman spectroscopy and trimodal wide-field imaging techniques for real-time in vivo tissue Raman measurements at endoscopy, Opt. Lett. 34 (2009) 758–760.

[38] M.G. Shim, B.C. Wilson, E. Marple, M. Wach, Study of fiber-optic probes for in vivo medical Raman spectroscopy, Appl. Spectrosc. 53 (1999) 619–627.

[39] L.F. Santos, R. Wolthuis, S. Koljenovic, R.M. Almeida, G.J. Puppels, Fiber-optic probes for in vivo Raman spectroscopy in the high-wavenumber region, Anal. Chem. 77 (2005) 6747–6752.

[40] S. Dochow, I. Latka, M. Becker, R. Spittel, J. Kobelke, K. Schuster, A. Graf, S. Brueckner, S. Unger, M. Rothhardt, B. Dietzek, C. Krafft, J. Popp, Multicore fiber with integrated fiber Bragg gratings for background-free Raman sensing, Opt. Express 20 (2012) 20156–20169.

[41] S. Koljenovic, T.C.B. Schut, R. Wolthuis, A.J.P.E. Vincent, G. Hendriks-Hagevi, L. Santos, J.M. Kros, G.J. Puppels, Raman spectroscopic characterization of porcine brain tissue using a single fiber-optic probe, Anal. Chem. 79 (2007) 557–564.

[42] S. Koljenovic, T.C.B. Schut, R. Wolthuis, B. de Jong, L. Santos, P.J. Caspers, J.M. Kros, G.J. Puppels, Tissue characterization using high wave number Raman spectroscopy, J. Biomed. Opt. 10 (2005).

[43] M. Kirsch, G. Schackert, R. Salzer, C. Krafft, Raman spectroscopic imaging for in vivo detection of cerebral brain metastases, Anal. Bioanal. Chem. 398 (2010) 1707–1713.

[44] C. Krafft, B. Belay, N. Bergner, B.F.M. Romeike, R. Reichart, R. Kalff, J.U. Popp, Advances in optical biopsy — correlation of malignancy and cell density of primary brain tumors using Raman microspectroscopic imaging, Analyst 137 (2012) 5533–5537.

[45] N. Bergner, A. Medyukhina, K.D. Geiger, M. Kirsch, G. Schackert, C. Krafft, J. Popp, Hyperspectral unmixing of Raman micro-images for assessment of morphological and chemical parameters in non-dried brain tumor specimens, Anal. Bioanal. Chem. 405 (2013) 8719–8728.

[46] O. Uckermann, R. Galli, S. Tamosaityte, E. Leipnitz, K.D. Geiger, G. Schackert, E. Koch, G. Steiner, M. Kirsch, Label-free delineation of brain tumors by coherent anti-stokes Raman scattering microscopy in an orthotopic mouse model and human glioblastoma, PLoS One 9 (2014).

[47] J.N. Bentley, M. Ji, X.S. Xie, D.A. Orringer, Real-time image guidance for brain tumor surgery through stimulated Raman scattering microscopy, Expert Rev. Anti-Infect. Ther. 14 (2014) 359–361.

[48] A. Medyukhina, T. Meyer, M. Schmitt, B.F.M. Romeike, B. Dietzek, J. Popp, Towards automated segmentation of cells and cell nuclei in nonlinear optical microscopy, J. Biophotonics 5 (2012) 878–888.

[49] M. Ji, D.A. Orringer, C.W. Freudiger, S. Ramkissoon, X. Liu, D. Lau, A.J. Golby, I. Norton, M. Hayashi, N.Y.R. Agar, G.S. Young, C. Spino, S. Santagata, S. Camelo-Piragua, K.L. Ligon, O. Sagher, X.S. Xie, Rapid, label-free detection of brain tumors with stimulated Raman scattering microscopy, Sci. Transl. Med. 5 (2013) (201ra119).

[50] J. Ferlay, P. Autier, M. Boniol, M. Heanue, M. Colombet, P. Boyle, Estimates of the cancer incidence and mortality in Europe in 2006, Ann. Oncol. 18 (2007) 581–592.

[51] I. Ellis, et al., Pathology Reporting of Breast Disease. A Joint Document Incorporating the Third Edition of the NHS Breast Screening Programme's Guidelines for Pathology Reporting in Breast Cancer Screening and the Second Edition of The Royal College of Pathologists' Minimum Dataset for Breast Cancer Histopathology, NHSBSP Publication, Sheffield, 2005.

[52] A.S. Haka, K.E. Shafer-Peltier, M. Fitzmaurice, J. Crowe, R.R. Dasari, M.S. Feld, Diagnosing breast cancer by using Raman spectroscopy, Proc. Natl. Acad. Sci. U. S. A. 102 (2005) 12371–12376.

[53] J. Kneipp, T.B. Schut, M. Kliffen, M. Menke-Pluijmers, G. Puppels, Characterization of breast duct epithelia: a Raman spectroscopic study, Vib. Spectrosc. 32 (2003) 67–74.

[54] N. Stone, P. Matousek, Advanced transmission Raman spectroscopy: a promising tool for breast disease diagnosis, Cancer Res. 68 (2008) 4424–4430.

[55] R. Baker, K.D. Rogers, N. Shepherd, N. Stone, New relationships between breast microcalcifications and cancer, Br. J. Cancer 103 (2010) 1034–1039.

[56] M.M. Kerssens, P. Matousek, K. Rogers, N. Stone, Towards a safe non-invasive method for evaluating the carbonate substitution levels of hydroxyapatite (HAP) in micro-calcifications found in breast tissue, Analyst 135 (2010) 3156–3161.

[57] A.S. Haka, Z. Volynskaya, J.A. Gardecki, J. Nazemi, R. Shenk, N. Wang, R.R. Dasari, M. Fitzmaurice, M.S. Feld, Diagnosing breast cancer using Raman spectroscopy: prospective analysis, J. Biomed. Opt. 14 (2009).

[58] Y. Yang, F. Li, L. Gao, Z. Wang, M.J. Thrall, S.S. Shen, K.K. Wong, S.T.C. Wong, Differential diagnosis of breast cancer using quantitative, label-free and molecular vibrational imaging, Biomed. Opt. Express 2 (2011) 2160–2174.

[59] J. Smith, C. Kendall, A. Sammon, J. Christie-Brown, N. Stone, Raman spectral mapping in the assessment of axillary lymph nodes in breast cancer, Technol. Cancer Res. Treat. 2 (2003) 327–331.

[60] J. Horsnell, P. Stonelake, J. Christie-Brown, G. Shetty, J. Hutchings, C. Kendall, N. Stone, Raman spectroscopy—a new method for the intra-operative assessment of axillary lymph nodes, Analyst 135 (2010) 3042–3047.

[61] CancerResearchUK, Survival statistics for the most common cancers, http://www.cancerresearchuk.org/cancer-info/cancerstats/survival/common-cancers/2014 (4/Nov/2014).

[62] J.K. Field, The screening imperative, Nature 513 (2014) S7-S7.

[63] Z.W. Huang, A. McWilliams, H. Lui, D.I. McLean, S. Lam, H.S. Zeng, Near-infrared Raman spectroscopy for optical diagnosis of lung cancer, Int. J. Cancer 107 (2003) 1047–1052.

[64] N.D. Magee, J.R. Beattie, C. Carland, R. Davis, K. McManus, I. Bradbury, D.A. Fennell, P.W. Hamilton, M. Ennis, J.J. McGarvey, J.S. Elborn, Raman microscopy in the diagnosis and prognosis of surgically resected nonsmall cell lung cancer, J. Biomed. Opt. 15 (2010).

[65] L. Gao, Z. Wang, F. Li, A.A. Hammoudi, M.J. Thrall, P.T. Cagle, S.T.C. Wong, Differential diagnosis of lung carcinoma with coherent anti-stokes Raman scattering imaging, Arch. Pathol. Lab. Med. 136 (2012) 1502–1510.

[66] J.X. Cheng, X.S. Xie, Coherent anti-Stokes Raman scattering microscopy: instrumentation, theory, and applications, J. Phys. Chem. B 108 (2004) 827–840.

[67] M.A. Short, S. Lam, A.M. McWilliams, D.N. Ionescu, H. Zeng, Using laser Raman spectroscopy to reduce false positives of autofluorescence bronchoscopies: a pilot study, J. Thorac. Oncol. 6 (2011) 1206–1214.

[68] CancerResearchUK, Skin Cancer Statistics, http://www.cancerresearchuk.org/cancer-info/cancerstats/types/skin/ (4/Nov/2014).

[69] AmericanCancerSociety, Figures Cancer Facts, http://www.cancer.org/acs/groups/content/@nho/documents/document/2008cafffinalsecuredpdf.pdf2008 (4/Nov/2014).

[70] C.A. Lieber, S.K. Majumder, D.L. Ellis, D.D. Billheimer, A. Mahadevan-Jansen, In vivo nonmelanoma skin cancer diagnosis using Raman microspectroscopy, Lasers Surg. Med. 40 (2008) 461–467.

[71] H. Lui, J. Zhao, D.I. McLean, H. Zeng, Real-time Raman spectroscopy for in vivo skin cancer diagnosis, Cancer Res. 72 (2012).

[72] K. Mosterd, G.A.M. Krekels, F.H.M. Nieman, J.U. Ostertag, B.A.B. Essers, C.D. Dirksen, P.M. Steijlen, A. Vermeulen, H.A.M. Neumann, N.W.J. Kelleners-Smeets, Surgical excision versus Mohs' micrographic surgery for primary and recurrent basal-cell carcinoma of the face: a prospective randomised controlled trial with 5-years' follow-up, Lancet Oncol. 9 (2008) 1149–1156.

[73] A. Nijssen, T.C.B. Schut, F. Heule, P.J. Caspers, D.P. Hayes, M.H.A. Neumann, G.J. Puppels, Discriminating basal cell carcinoma from its surrounding tissue by Raman spectroscopy, J. Invest. Dermatol. 119 (2002) 64–69.

[74] N. Vogler, T. Meyer, D. Akimov, I. Latka, C. Krafft, N. Bendsoe, K. Svanberg, B. Dietzek, J. Popp, Multimodal imaging to study the morphochemistry of basal cell carcinoma, J. Biophotonics 3 (2010) 728–736.

[75] S. Heuke, N. Vogler, T. Meyer, D. Akimov, F. Kluschke, H.J. Roewert-Huber, J. Lademann, B. Dietzek, J. Popp, Multimodal mapping of human skin, Br. J. Dermatol. 169 (2013) 794–803.

[76] A. Medyukhina, T. Meyer, S. Heuke, N. Vogler, B. Dietzek, J. Popp, Automated seeding-based nuclei segmentation in nonlinear optical microscopy, Appl. Opt. 52 (2013) 6979–6994.

[77] C. Kendall, N. Stone, N. Shepherd, K. Geboes, B. Warren, R. Bennett, H. Barr, Raman spectroscopy, a potential tool for the objective identification and classification of neoplasia in Barrett's oesophagus, J. Pathol. 200 (2003) 602–609.

[78] T.C. Bakker Schut, M.J. Witjes, H.J. Sterenborg, O.C. Speelman, J.L. Roodenburg, E.T. Marple, H.A. Bruining, G.J. Puppels, In vivo detection of dysplastic tissue by Raman spectroscopy, Anal. Chem. 72 (2000) 6010–6018.

[79] M.G. Shim, L. Song, N.E. Marcon, B.C. Wilson, In vivo near-infrared Raman spectroscopy: demonstration of feasibility during clinical gastrointestinal endoscopy, Photochem. Photobiol. 72 (2000) 146–150.

[80] L.-M. Wong Kee Song, B.C. Wilson, Best Pract. Res. Clin. Gastroenterol. 19 (2005) 833–856.

[81] M.S. Bergholt, W. Zheng, K. Lin, K.Y. Ho, M. Teh, K.G. Yeoh, J.B.Y. So, Z. Huang, In vivo diagnosis of esophageal cancer using image-guided raman endoscopy and biomolecular modeling, Technol cancer res t 10 (2011) 103–112.

[82] S.K. Teh, W. Zheng, K.Y. Ho, M. Teh, K.G. Yeoh, Z. Huang, Diagnostic potential of near-infrared Raman spectroscopy in the stomach: differentiating dysplasia from normal tissue, Br. J. Cancer 98 (2008) 457–465.

[83] L.M. Almond, J. Hutchings, G. Lloyd, H. Barr, N. Shepherd, J. Day, O. Stevens, S. Sanders, M. Wadley, N. Stone, C. Kendall, Endoscopic Raman spectroscopy enables objective diagnosis of dysplasia in Barrett's esophagus, Gastrointest. Endosc. 79 (2014) 37–45.

[84] G. Shetty, C. Kendall, N. Shepherd, N. Stone, H. Barr, Raman spectroscopy: elucidation of biochemical changes in carcinogenesis of oesophagus, Br. J. Cancer 94 (2006) 1460–1464.

[85] J. Hutchings, C. Kendall, N. Shepherd, H. Barr, N. Stone, Evaluation of linear discriminant analysis for automated Raman histological mapping of esophageal high-grade dysplasia, J. Biomed. Opt. 15 (2010).

[86] P. Crow, N. Stone, C.A. Kendall, J.S. Uff, J.A.M. Farmer, H. Barr, M.P.J. Wright, The use of Raman spectroscopy to identify and grade prostatic adenocarcinoma in vitro, Br. J. Cancer 89 (2003) 106–108.

[87] N. Stone, M.C.H. Prieto, P. Crow, J. Uff, A.W. Ritchie, The use of Raman spectroscopy to provide an estimation of the gross biochemistry associated with urological pathologies, Anal. Bioanal. Chem. 387 (2007) 1657–1668.

[88] P. Crow, A. Molckovsky, N. Stone, J. Uff, B. Wilson, L.M. Wongkeesong, Assessment of fiberoptic near-infrared Raman spectroscopy for diagnosis of bladder and prostate cancer, Urology 65 (2005) 1126–1130.

[89] P. Crow, B. Barrass, C. Kendall, M. Hart-Prieto, M. Wright, R. Persad, N. Stone, The use of Raman spectroscopy to differentiate between different prostatic adenocarcinoma cell lines, Br. J. Cancer 92 (2005) 2166–2170.

[90] D.S. Grubisha, R.J. Lipert, H.Y. Park, J. Driskell, M.D. Porter, Femtomolar detection of prostate-specific antigen: an immunoassay based on surface-enhanced Raman scattering and immunogold labels, Anal. Chem. 75 (2003) 5936–5943.

[91] R.E. Kast, S.C. Tucker, K. Killian, M. Trexler, K.V. Honn, G.W. Auner, Emerging technology: applications of Raman spectroscopy for prostate cancer, Cancer Metastasis Rev. 33 (2014) 673–693.

[92] J.C. Taylor, C.A. Kendall, N. Stone, T.A. Cook, Optical adjuncts for enhanced colonoscopic diagnosis, Brit. J. Surg. 94 (2007) 6–16.

[93] R.S. DaCosta, B.C. Wilson, N.E. Marcon, Optical techniques for the endoscopic detection of dysplastic colonic lesions, Curr. Opin. Gastroenterol. 21 (2005) 70–79.

[94] A. Molckovsky, L. Song, M.G. Shim, N.E. Marcon, B.C. Wilson, Diagnostic potential of near-infrared Raman spectroscopy in the colon: differentiating adenomatous from hyperplastic polyps, Gastrointest. Endosc. 57 (2003) 396–402.

[95] E. Widjaja, W. Zheng, Z. Huang, Classification of colonic tissues using near-infrared Raman spectroscopy and support vector machines, Int. J. Oncol. 32 (2008) 653–662.

[96] A. Taketani, R. Hariyani, M. Ishigaki, B.B. Andriana, H. Sato, Raman endoscopy for the in situ investigation of advancing colorectal tumors in live model mice, Analyst 138 (2013) 4183–4190.

[97] M.A. Short, I.T. Tai, D. Owen, H. Zeng, Using high frequency Raman spectra for colonic neoplasia detection, Opt. Express 21 (2013) 5025–5034.

[98] G.R. Lloyd, J. Wood, C. Kendall, T. Cook, N. Shepherd, N. Stone, Histological imaging of a human colon polyp sample using Raman spectroscopy and self organising maps, Vib. Spectrosc. 60 (2012) 43–49.

[99] I. Rehman, R. Smith, L.L. Hench, W. Bonfield, Structural evaluation of human and sheep bone and comparison with synthetic hydroxyapatite by FT-Raman spectroscopy, J. Biomed. Mater. Res. 29 (1995) 1287–1294.

[100] M.D. Morris, G.S. Mandair, Raman assessment of bone quality, Clin. Orthop. Relat. Res. 469 (2011) 2160–2169.

[101] J.G. Kerns, P.D. Gikas, K. Buckley, A. Shepperd, H.L. Birch, I. McCarthy, J. Miles, T.W.R. Briggs, R. Keen, A.W. Parker, P. Matousek, A.E. Goodship, Evidence from Raman spectroscopy of a putative link between inherent bone matrix chemistry and degenerative Joint disease, Arthritis Rheum. 66 (2014) 1237–1246.

[102] M.V. Schulmerich, W.F. Finney, V. Popescu, M.D. Morris, T.M. Vanasse, S.A. Goldstein, Transcutaneous Raman spectroscopy of bone tissue using a non-confocal fiber optic array probe — art. no. 60930O, in: A. MahadevanJansen, W.H. Petrich (Eds.),Biomedical Vibrational Spectroscopy III: Advances in Research and Industry, 2006.

[103] B.R. McCreadie, M.D. Morris, T.-c. Chen, D.S. Rao, W.F. Finney, E. Widjaja, S.A. Goldstein, Bone tissue compositional differences in women with and without osteoporotic fracture, Bone 39 (2006) 1190–1195.

[104] D.M. Good, V. Thongboonkerd, J. Novak, J.-L. Bascands, J.P. Schanstra, J.J. Coon, A. Dominiczak, H. Mischak, Body fluid proteomics for biomarker discovery: lessons from the past hold the key to success in the future, J. Proteome Res. 6 (2007) 4549–4555.

[105] J. Filik, N. Stone, Drop coating deposition Raman spectroscopy of protein mixtures, Analyst 132 (2007) 544–550.

[106] J. Filik, N. Stone, Analysis of human tear fluid by Raman spectroscopy, Anal. Chim. Acta 616 (2008) 177–184.

[107] J. Filik, N. Stone, Investigation into the protein composition of human tear fluid using centrifugal filters and drop coating deposition Raman spectroscopy, J. Raman Spectrosc. 40 (2009) 218–224.

[108] D. Rohleder, W. Kiefer, W. Petrich, Quantitative analysis of serum and serum ultrafiltrate by means of Raman spectroscopy, Analyst 129 (2004) 906–911.

[109] D. Qi, A.J. Berger, Chemical concentration measurement in blood serum and urine samples using liquid-core optical fiber Raman spectroscopy, Appl. Opt. 46 (2007) 1726–1734.

[110] K.E. Shafer-Peltier, C.L. Haynes, M.R. Glucksberg, R.P. Van Duyne, Toward a glucose biosensor based on surface-enhanced Raman scattering, J. Am. Chem. Soc. 125 (2003) 588–593.

[111] C.L. Haynes, R.P. Van Duyne, Plasmon-sampled surface-enhanced Raman excitation spectroscopy, J. Phys. Chem. B 107 (2003) 7426–7433.

[112] J.M. Yuen, N.C. Shah, J.T. Walsh Jr., M.R. Glucksberg, R.P. Van Duyne, Transcutaneous glucose sensing by surface-enhanced spatially offset Raman spectroscopy in a rat model, Anal. Chem. 82 (2010) 8382–8385.

[113] J. Lin, Y. Zeng, J. Lin, J. Wang, L. Li, Z. Huang, B. Li, H. Zeng, R. Chen, Erythrocyte membrane analysis for type II diabetes detection using Raman spectroscopy in high-wavenumber region, Appl. Phys. Lett. 104 (2014).

[114] S.K. Jain, R. McVie, J. Duett, J.J. Herbst, Erythrocyte membrane lipid peroxidation and glycosylated hemoglobin in diabetes, Diabetes 38 (1989) 1539–1543.

[115] T.J. Harvey, E.C. Faria, A. Henderson, E. Gazi, A.D. Ward, N.W. Clarke, M.D. Brown, R.D. Snook, P. Gardner, Spectral discrimination of live prostate and bladder cancer cell lines using Raman optical tweezers, J. Biomed. Opt. 13 (2008).

[116] T.J. Harvey, C. Hughes, A.D. Ward, E.C. Faria, A. Henderson, N.W. Clarke, M.D. Brown, R.D. Snook, P. Gardner, Classification of fixed urological cells using Raman tweezers, J. Biophotonics 2 (2009) 47–69.

[117] I. Taleb, G. Thiefin, C. Gobinet, V. Untereiner, B. Bernard-Chabert, A. Heurgue, C. Truntzer, P. Hillon, M. Manfait, P. Ducoroy, G.D. Sockalingum, Diagnosis of hepatocellular carcinoma in cirrhotic patients: a proof-of-concept study using serum micro-Raman spectroscopy, Analyst 138 (2013) 4006–4014.

[118] J.L. Pichardo-Molina, C. Frausto-Reyes, O. Barbosa-Garcia, R. Huerta-Franco, J.L. Gonzalez-Trujillo, C.A. Ramirez-Alvarado, G. Gutierrez-Juarez, C. Medina-Gutierrez, Raman spectroscopy and multivariate analysis of serum samples from breast cancer patients, Lasers Med. Sci. 22 (2007) 229–236.

[119] A.T. Harris, A. Lungari, C.J. Needham, S.L. Smith, M.A. Lones, S.E. Fisher, X.B. Yang, N. Cooper, J. Kirkham, D.A. Smith, D.P. Martin-Hirsch, A.S. High, Potential for Raman spectroscopy to provide cancer screening using a peripheral blood sample, Head Neck Oncol. 1 (2009).

[120] J.W. Chan, D.S. Taylor, T. Zwerdling, S.M. Lane, K. Ihara, T. Huser, Micro-Raman spectroscopy detects individual neoplastic and normal hematopoietic cells, Biophys. J. 90 (2006) 648–656.

[121] J.W. Chan, D.S. Taylor, S.M. Lane, T. Zwerdling, J. Tuscano, T. Huser, Nondestructive identification of individual leukemia cells by laser trapping Raman spectroscopy, Anal. Chem. 80 (2008) 2180–2187.

[122] C.M. MacLaughlin, N. Mullaithilaga, G. Yang, S.Y. Ip, C. Wang, G.C. Walker, Surface-enhanced Raman scattering dye-labeled Au nanoparticles for triplexed detection of leukemia and lymphoma cells and SERS flow cytometry, Langmuir 29 (2013) 1908–1919.

[123] S. Li, Y. Zhang, J. Xu, L. Li, Q. Zeng, L. Lin, Z. Guo, Z. Liu, H. Xiong, S. Liu, Noninvasive prostate cancer screening based on serum surface-enhanced Raman spectroscopy and support vector machine, Appl. Phys. Lett. 105 (2014).

[124] S. Dochow, C. Beleites, T. Henkel, G. Mayer, J. Albert, J. Clement, C. Krafft, J. Popp, Quartz microfluidic chip for tumour cell identification by Raman spectroscopy in combination with optical traps, Anal. Bioanal. Chem. 405 (2013) 2743–2746.

[125] S. Dochow, C. Krafft, U. Neugebauer, T. Bocklitz, T. Henkel, G. Mayer, J. Albert, J. Popp, Tumour cell identification by means of Raman spectroscopy in combination with optical traps and microfluidic environments, Lab Chip 11 (2011) 1484–1490.

[126] A. Sahu, K. Dalal, S. Naglot, P. Aggarwal, C.M. Krishna, Serum based diagnosis of asthma using Raman spectroscopy: an early phase pilot study, PLoS One 8 (2013).

[127] M.S. Bergholt, S. Hassing, Quantification of C-Reactive protein in human blood plasma using near-infrared Raman spectroscopy, Analyst 134 (2009) 2123–2127.

[128] U. Neugebauer, S. Trenkmann, T. Bocklitz, D. Schmerler, M. Kiehntopf, J. Popp, Fast differentiation of SIRS and sepsis from blood plasma of ICU patients using Raman spectroscopy, J. Biophotonics 7 (2014) 232–240.

[129] K.W.C. Poon, F.M. Lyng, P. Knief, O. Howe, A.D. Meade, J.F. Curtin, H.J. Byrne, J. Vaughan, Quantitative reagent-free detection of fibrinogen levels in human blood plasma using Raman spectroscopy, Analyst 137 (2012) 1807–1814.

[130] A.M.T. Monfared, V.S. Tiwari, M.M. Tripathi, H. Anis, Raman spectroscopy for clinical-level detection of heparin in serum by partial least-squares analysis, J. Biomed. Opt. 18 (2013).

[131] C.J. Murray, L.C. Rosenfeld, S.S. Lim, K.G. Andrews, K.J. Foreman, D. Haring, N. Fullman, M. Naghavi, R. Lozano, A.D. Lopez, Global malaria mortality between 1980 and 2010: a systematic analysis, Lancet 379 (2012) 413–431.

[132] A. Bonifacio, S. Finaurini, C. Krafft, S. Parapini, D. Taramelli, V. Sergo, Spatial distribution of heme species in erythrocytes infected with *Plasmodium falciparum* by use of resonance Raman imaging and multivariate analysis, Anal. Bioanal. Chem. 392 (2008) 1277–1282.

[133] B.R. Wood, D. McNaughton, Raman excitation wavelength investigation of single red blood cells in vivo, J. Raman Spectrosc. 33 (2002) 517–523.

[134] A.J. Hobro, A. Konishi, C. Coban, N.I. Smith, Raman spectroscopic analysis of malaria disease progression via blood and plasma samples, Analyst 138 (2013) 3927–3933.